Journal of Materials Processing Technology 221 (2015) 100–111

Contents lists available at ScienceDirect

Journal of Materials Processing Technology

journal homepage: www.elsevier.com/locate/jmatprotec

Deformation mechanics and efficient force prediction in single point incremental forming

Yanle Li*, William J.T. Daniel, Zhaobing Liu, Haibo Lu, Paul A. Meehan

School of Mechanical & Mining Engineering, The University of Queensland, St Lucia, Brisbane 4072, QLD, Australia

ARTICLE INFO

Article history:
Received 25 August 2014
Received in revised form
23 November 2014
Accepted 7 February 2015
Available online 16 February 2015

Keywords:
Incremental sheet forming
Forming force
Deformation mechanics
Prediction
Shear
Bending

ABSTRACT

Incremental sheet forming (ISF) is a promising forming process which is able to deform a flat sheet into a complex 3D shape by using a generic moving tool. The flexibility, increased formability and the reduced forming force make the ISF process ideal for rapid prototype and small batch production. However, the effective production design and optimization in ISF require the efficient prediction of forming force, especially the tangential force which is the actual force component that does plastic work during the forming process. In this paper, in order to investigate the deformation mechanism in the ISF process, a comprehensive finite element (FE) model for the cone-forming process with fine solid elements is established which allows the quantitative study of the deformation behavior of stretching, bending and shearing during the process. Based on such analysis, an efficient model for tangential force prediction is deduced analytically in which all these three deformation modes are considered. In particular, the contribution from each deformation mode is related to the variation of forming parameters. Additionally, the proposed efficient model is comprehensively validated with both truncated cone and pyramid shapes by varying four forming parameters (i.e. step down, wall angle, tool radius and sheet thickness). In both cases, the predicted forces show good agreements with the experimental results. Furthermore, the proposed model is generalized to deal with more complex shapes (e.g. ellipsoidal cup). It is found that the trend of tangential force could be properly represented by the change of the curvature of the formed part. Considering the proposed model can be solved within only several minutes, it will guide the forming process and shorten the lead time.

1. Introduction

Incremental sheet forming (ISF) is an extremely flexible process using a single generic tool for an infinite variety of shapes with great potential for production of short runs of new or replacements parts. By using this process, useable parts can be formed directly from CAD data with a minimum of specialized tooling; therefore, it has a high potential and economic payoff for rapid prototyping and small quantity production for various applications. In the early stage of the ISF technology, Allwood et al. (2005) performed a structured search which identified the potential applications; Ambrogio et al. (2005) successfully produced a customized ankle support with good dimensional accuracy; Micari et al. (2007) demonstrated that ISF can be used for manufacturing automotive body parts. However, the further development and commercialization of ISF is presently inhibited by a lack of understanding in the deformation mechanics. In particular, a model-based efficient prediction of forming force is critical to improve the production efficiency as it provides monitoring of the forming process, failure prediction, and a future means of on-line control and optimization.

Over the last decade, the deformation mechanics behind ISF is investigated both analytically and experimentally. Silva et al. (2008) extensively analyzed the single-point incremental forming by considering membrane strains. A closed-form analytical model is first presented which provides insight to explain the fundamentals behind the fracture of material and the enhanced overall formability of ISF. Emmens and Boogaard (2008) summarized that bending under tensile load plays a critical role in the localized deformation of the ISF process. Additionally, using finite element (FE) simulation, Smith et al. (2013) demonstrated the deformation mechanics in single point incremental forming and compared with that in accumulative double-sided incremental forming process. Lu et al. (2014) further discussed the role of friction and through-thickness-shear analytically from the stress state point of view. It was claimed that through-thickness-shear caused by friction results in contrary effects on deformation stability and formability. Through

* Corresponding author. Tel.: +61 3365 4115.
E-mail addresses: yanle.li@uq.edu.au, kuge0501@126.com (Y. Li).

http://dx.doi.org/10.1016/j.jmatprotec.2015.02.009
0924-0136/

experimental measurements, Jackson and Allwood (2009) found that the deformation mechanism in ISF is a combination of stretching and shear in the plane perpendicular to the tool motion but shear in the tool direction. However, Eyckens et al. (2011) suggested that the dominant deformation mechanism depends on the selected forming parameters (e.g. wall angle, step-down size and spindle rotation speed).

On the one hand, forming forces during ISF have been experimentally studied intensively. Duflou et al. (2007) concluded that the forming forces are increased with the increase of vertical step down size, wall angle and sheet thickness. Filice et al. (2006) worked on the force analysis and classified the force trends of tangential force into three types: steady state force trends, polynomial force trends and monotonically decreasing force trends. Ambrogio et al. (2006) found that the force gradient after the peak can be effectively considered as a critical indicator to detect and prevent work piece fracture. Filice et al. (2006) considered forming force as an indicator to realize the on-line control and optimization. Petek et al. (2009) proposed an autonomous on-line system for fracture identification and localization by analyzing the reaction force with a skewness function. Another failure criterion presented by Fiorentino (2013) is also based on force monitoring during the forming process. Additionally, Ingarao et al. (2012) evaluated the energy consumption required for the ISF process according to the measured force data, which provides guidance for sustainable development of the process. However, very limited analytical models are available for the efficient prediction of forming forces in ISF although some researchers have attempted to bridge this gap. Due to the localized contact condition and long tool path in ISF, force prediction with FE models is significantly time-consuming, although it is commonly used for various forming processes. Smith et al. (2013) reported a simulation time of 24 days for a single point incremental forming process for a truncated cone shape. To overcome the above computational challenges of the FE approach, Iseki (2001) obtained the forming forces for the incremental forming of a pyramid using a simple approximated deformation analysis based on a plane-strain deformation. Raithatha and Duncan (2009) developed a model based on the numerical minimization of internal work within the material. In this method, the minimization of plastic work was formulated as a Second Order Cone Programming (SOCP) optimization problem. By sacrificing the accuracy, a process of straight line indentation on a sheet with dimensions of 0.1 m × 0.1 m is achieved in 9 min. Aerens et al. (2010) studied the incremental forming of truncated cones with different materials using experimental and statistical analyses. Regression formulae were proposed to predict the triple forming forces including axial, radial, and tangential components from input variables including wall angle, initial thickness, tool diameter, and vertical pitch. In particular, the tangential force is the actual force component that does plastic work during the forming process, so it is more closely related to the deformation mechanism of the process. Also, the prediction of the tangential component could contribute as a pathway for the extensive investigation of both vertical and radial components. In addition, although the value of the tangential force tends to be small compared with vertical force, the trend of the tangential force might be used as an important potential indicator for preventing material failure and to hence enhance the surface quality. Recently, Mirnia and Dariani (2012) conducted an upper-bound analysis to predict the tangential force on a truncated cone-forming process using an assumed deformation zone. It was reported that the forces were in good agreement with those from the experimental work of Aerens et al. (2010). Nevertheless, large errors can be expected for severe deformation conditions (e.g. $\Delta z > 0.5$ mm) and possibly due to the pure shearing assumption of plastic deformation.

Li et al. (2014b) have proposed a preliminary efficient force prediction model with validation by forming of truncated cone shapes. Even though the model shows great potential to deal with various process parameters, it uses empirical coefficients to combine different deformation modes that require further quantitative investigation and experimental validation. Additionally, a generalized model that can be used in any user-defined shapes is required. In particular, this paper will focus on the further extension and validation of the efficient force prediction model. The main contributions of this paper to the field are:

- It is clarified that the deformation mechanics in the cone-forming ISF process involves shearing, stretching and bending through a FE simulation.
- An efficient tangential force prediction model is proposed which takes into account the above three deformation modes. The model is comprehensively validated with two benchmark shapes (truncated cone and pyramid) with varying forming parameters including step-down size, wall angle, tool diameter and sheet thickness.
- The proposed model is successfully extended and validated for a more complex shape (i.e. ellipsoidal cup) by considering the change of local curvature. This will provide a valuable contribution towards the future investigation for the force prediction of general shapes.

2. FE model for deformation analysis

The understanding of the deformation mechanism in ISF is fundamental for the establishment of the analytical model for the prediction of forming force. However, it is difficult to reveal the detailed deformation history behind the ISF solely through experimental works due to its highly localized characteristic. Specifically, FE simulations can allow individual quantitative investigations of stretching, bending and shearing strains which are difficult to achieve using an experimental approach. Another benefit of FE simulations is that working parameters can be efficiently adjusted without any considerable economic cost. Therefore, computer models especially FE technology is widely applied to investigate this process. In particular, the explicit FE code of LS-DYNA is used in the present study due to its great performance to solve dynamic problems with large plastic deformation.

2.1. FE modelling

In the presented FE model, the forming tool is considered as a rigid body and its movement follows the same tool path as in the actual forming process which was designed using CAM software. As shown in Fig. 1 (revised from Silva et al., 2008), the truncated cone is formed in a stepwise way with a series of contours. The vertical distance between each neighbouring contour is defined as step-down size Δz and the angle between the deformed sheet to the horizontal plane is defined as wall angle α.

To accurately predict the through thickness shear and bending effect of the deformed sheet, the element type of SOLID164 is used in the current model and five elements are meshed through the thickness direction. The initial meshing configuration of the metal sheet is shown in Fig. 2 with an enlarged view of the selected small region d plotted at the top right corner. In particular, for the region which will be contacting with the tool (region B), the elements are arranged with the size equal to 1 mm radially and meshed into 400 elements circumferentially which correspond to the size between 0.7 mm to 1.2 mm. The general geometry of the sheet is square with dimension 300 mm × 300 mm and thus it is meshed with 175,000 solid elements. In terms of the boundary conditions in the forming process, nodes belong to the four edges of the squared sheet are constrained in all degrees of freedom.

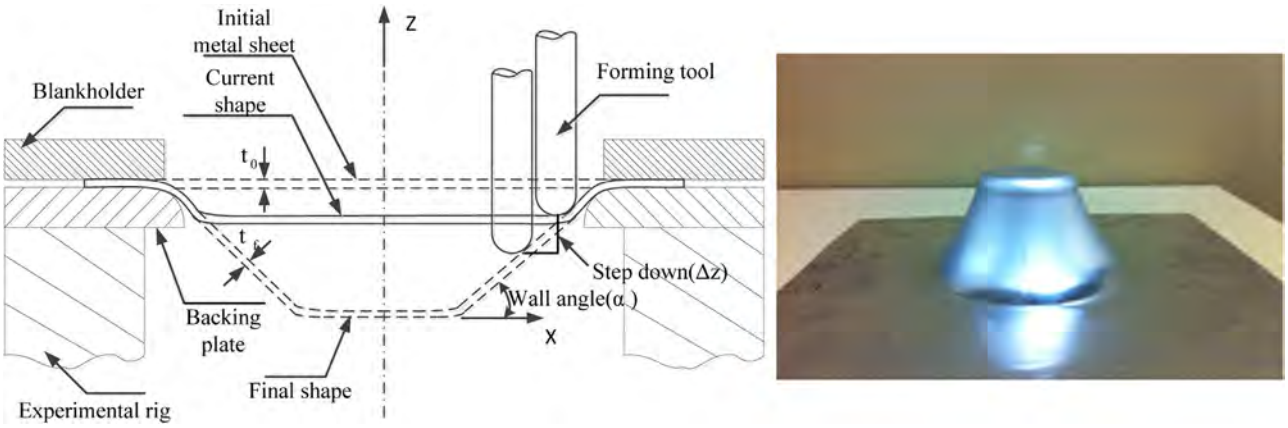

Fig. 1. Sketch of ISF experimental parameters and a case study made from Al 7075 of 1.6 mm in thickness (refer to Silva et al., 2008).

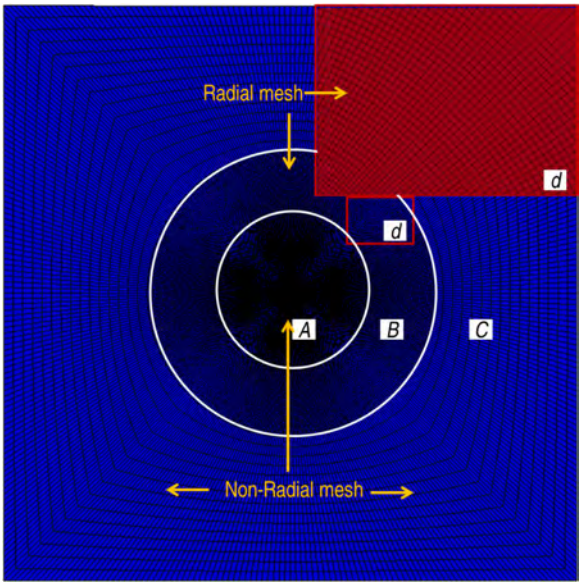

Fig. 2. The initial meshing configuration of the metal sheet with an enlarged view at the right top corner.

The metal used is the aluminum alloy 7075-O sheet with a thickness of 1.6 mm. It is confirmed from tensile tests that the material can be considered isotropic since deviations of the stress–strain behavior in different directions (rolling, diagonal and transverse) are small. Therefore, the material could be modeled using Swift's isotropic strain hardening law of $\sigma = K(\varepsilon_0 + \varepsilon)^n$. The detailed mechanical parameters are listed in Table 1 which were determined from previous material testing in Liu et al. (2013). From our previous experimental work, Li et al. (2014a), the friction at the contact surface between tool head and sheet has been assessed with a value of 0.18. This value has been used in this FE model. In order to improve the simulation efficiency, the virtual forming speed is scaled up by 100 times in which the ratio of the kinetic energy to the total internal energy can be controlled within 1% to ensure a quasi-static forming process.

Table 1
Mechanical properties of Aluminium 7075-O sheets with 1.6 mm thickness.

Material	7075-O
Density (t/mm^{-3})	2.81×10^{-9}
Young's modulus (GPa)	70
Poisson's ratio	0.33
Tensile yield strength (MPa)	92
Ultimate tensile strength (MPa)	198
Plastic coefficient K	352.58
Hardening exponent n	0.221

2.2. FE simulation results

Fig. 3 shows the deformed sheet on a cross-section perpendicular to the forming direction as well as the top view from the FE simulation. The displacement of elements in the vertical direction (Z) is presented with colored contours. In particular, strain components at the Section A are selected to have further investigation as the forming tool has already passed this section and reached a relatively steady state. Despite the fact that the maximum forming force occurs during contacting with elements, it is hard to observe the strain behavior of elements as it undergoes a transition period. Due to the inherent localized feature of ISF, the strain state of the

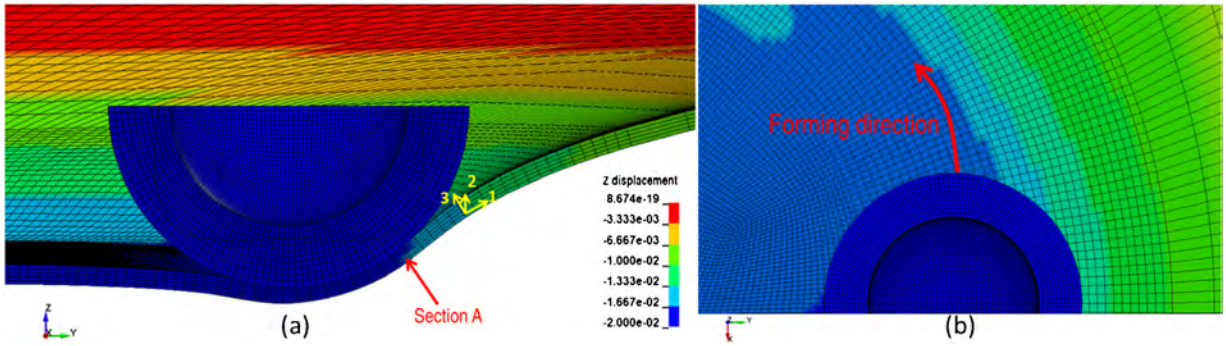

Fig. 3. Deformed sheet in the FE model: (a) cross-sectional view perpendicular to the forming direction and (b) top view.

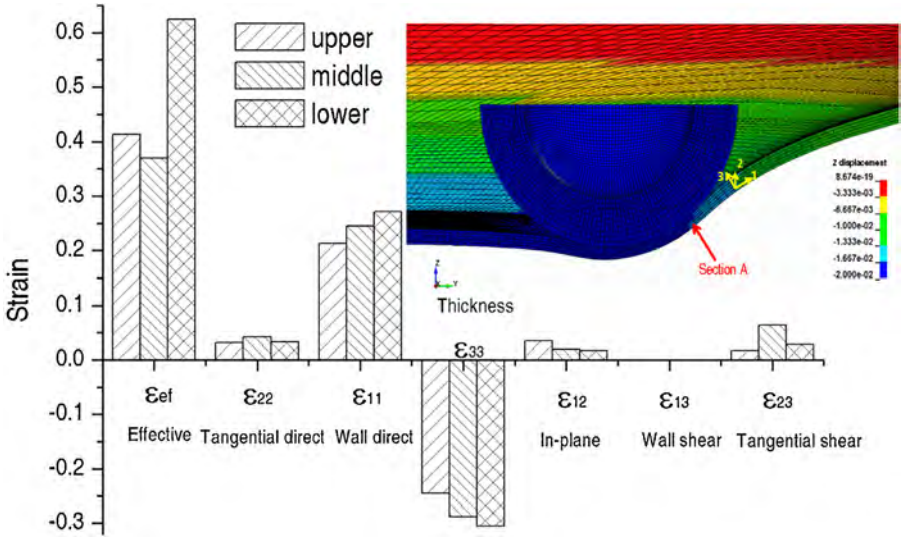

Fig. 4. Strain components for upper, middle and lower elements at Section A at the forming depth of 20 mm.

deformed elements will not be considerable affected by the following move of the forming tool. Furthermore, strain values along thickness direction are also investigated by checking upper element (the side in contact with the forming tool), lower element (the side without contact with the forming tool) and the middle element. It should be noted that the following strain values are presented in the local Cartesian coordinate system as marked in Fig. 3: the direction perpendicular to the tool motion and along the inclined wall is defined as 1 while forming direction (tangential direction) is defined as 2 and thickness direction as 3.

Since the strain components in ISF were developed incrementally, it is reasonable to analyze these values at a certain depth for comparison purpose. Such a comparison is presented in Fig. 4 as a bar graph for upper, middle and lower elements at Section A. These values are obtained when the forming tool is at the depth of 20 mm. It is noted that the strain component perpendicular to the forming direction and along the inclined wall (ε_{11} wall strain) dominates the total plastic strain at the selected elements with the highest positive strain. According to the law of volume constancy, the sheet has to be thinned during this process which is clearly confirmed by the negative thickness strain (ε_{33}) in Fig. 4. Not surprisingly, the direct strain values in the forming direction (ε_{22}) are small compared with the other two orthogonal directions as the deformation in this direction is symmetrical and constrained for extension. In contrast, shear strain in the forming direction ε_{23} prevails greatly among the three shear components, whereas the value of ε_{13} is negligible. The above results from FE simulation agree with the experimental measurement by Jackson and Allwood (2009). It is also noticed that the strain values are varying through the thickness as shown in Fig. 4. The lower element on the non-contacting surface was deformed with the highest effective strain value which is mainly resulted from the large strain ε_{11} and thickness strain ε_{33}. It should be noticed that the in-plane shear strain ε_{12} takes a non-negligible role to contribute to the substantial effective strain value especially for the upper element. The above detailed analysis indicates that the deformation mechanism is different between the forming and its perpendicular directions. More specifically, the deformation mode in the circumferential direction is a combination of the transverse shear strain ε_{23} and also a comparable amount of direct strain ε_{22}. However, the direct strain ε_{11} governs the deformation behavior in the direction perpendicular to the tool motion. This confirms that the formation of the inclined wall is represented by a combination of stretching and bending effect with non-negligible transverse shear in the current cone shape.

3. Analytical model for force prediction

For many metal-working processes, including incremental sheet forming, no exact analytical solutions for the forces to cause unconstrained plastic deformation are available as claimed by Hosford and Caddell (2007). This is because the exact solutions must be both statically and kinematically admissible which means that the solutions must be geometrically self-consistent as well as satisfying the required stress equilibrium everywhere in the deforming body. To this end, based on previous work by Mirnia and Dariani (2012), the upper bound theorem stated in Johnson and Mellor (1983) is adopted in the ISF process. This analysis is based on satisfying yield criteria and geometric self-consistency but not necessarily satisfying the stress equilibrium. According to the principle of maximum work dissipation, in a given set of strain increment field, the plastic work due to the true increment is greater than the same strain increment by any other distribution of stresses which conforms to the same yield criterion. Therefore, the estimated force based on the upper-bound theorem by equating the rate of internal energy dissipation to the external forces will equal or be greater than the actual one. In the analysis, the following assumptions have to be made: (i) the material is homogeneous and isotropic; (ii) interfaces are frictionless; and (iii) the material is rigid except in the deformation zone. To summarize, the calculation involves the following four steps for the prediction of tangential force in a cone-forming process.

1. Define an internal flow field and discretise the deformation zone into smaller regions. A kinematically admissible displacement field of the deformed surface ahead of the forming tool is represented by two adjustable parameters *M* and *N*.
2. Derive the velocity fields for each region from the assumed displacement field based on different plastic deformation conditions.
3. Calculate the strain rates and the dissipated power of the forming process due to different deformation modes.
4. Minimize the dissipated power by varying two parameters in their defined range. Consequently, forming force can be calculated by equating the rate of external work with the rate of internal dissipated power.

Two modules based on different deformation mechanisms (shear and bending with stretching) are included in the proposed

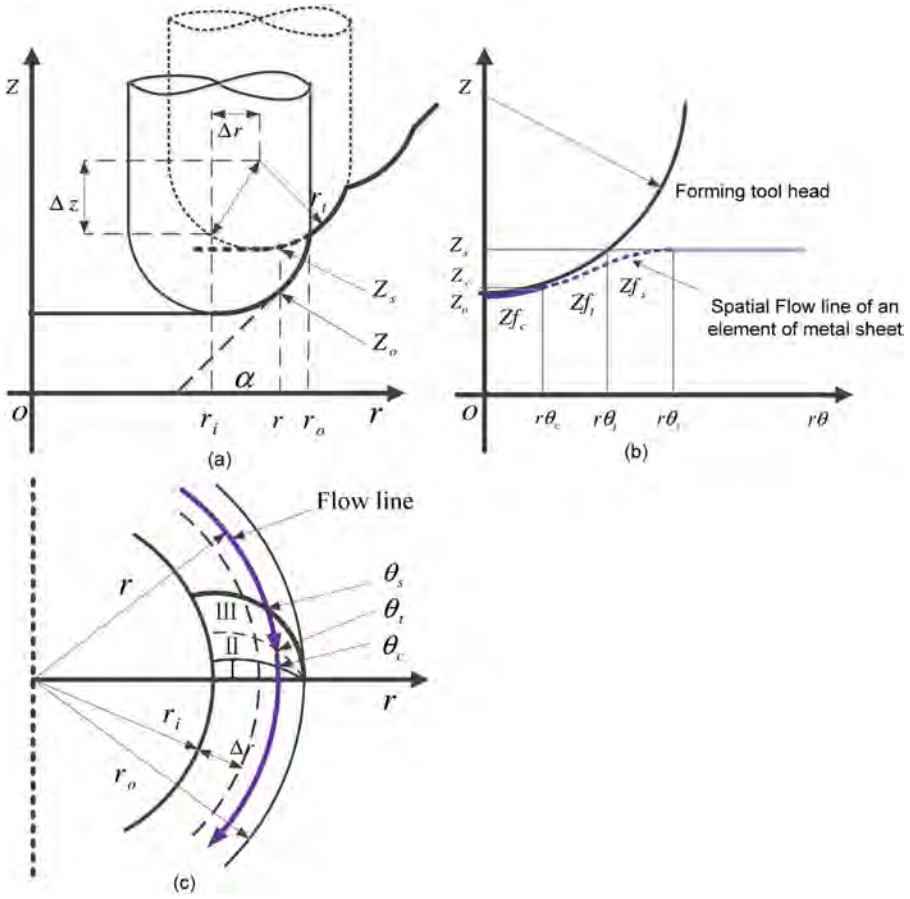

Fig. 5. Deformation zone in the cone forming process: (a) r–z view of the geometrical relations in incremental sheet forming during previous and current path, (b) $r\theta - z$ view of a typical flow line for the deformed curved surface along the circumferential direction of the sheet ahead of the tool and (c) $r - \theta$ view.

model to represent the effects due to the variation of forming parameters. Fig. 5 shows the deformation zone in the ISF process from different viewing aspects. Parameters used for the analytical formulation are defined in Fig. 5 and the similar division of the deformation zone could be found in the published work by Li et al. (2014b) and Mirnia and Dariani (2012). A kinematically admissible displacement field is assumed for the deformed surface ahead of the forming tool. This deformed surface Zf is represented by a series of flow lines along circumferential direction which can be tailored by adjusting two presupposed parameters M and N.

$$Zf = \begin{cases} Zf_c\left(r,\theta\right) = Z_t & \left(0 \le \theta \le \theta_c\right) \\ Zf_t\left(r,\theta\right) = S(X) \times Z_t & \left(\theta_c \le \theta \le \theta_t\right) \\ Zf_s\left(r,\theta\right) = S(X) \times Z_s & \left(\theta_t \le \theta \le \theta_s\right) \end{cases}. \tag{1}$$

Here Z_t is the geometric function of the tool surface and the boundary position is defined using M and Z_s represents the vertical height of the sheet after the previous pass (refer Fig. 5). $S(X)$ is tentatively designed as two-second order Bezier curves ranging from 0 to 1 which depends on N. More detailed calculation procedure for determining the position of the flow line is given in Appendix A. As a result, it is effective to adjust the deformed surface with parameters M and N. However, a velocity discontinuity surface is introduced at the intersecting surface of Zf_t and Zf_s which will result in extra dissipated power.

The following equations summarized the published work, Li et al. (2014b), regarding the calculation of dissipated powers due to three different deformation modes and also the velocity discontinuity surface. The dissipated power of the flow line during the cone forming process based on the shear deformation is integrated using strain rates over the deformed surface as

$$\dot{w}_f = y_0 \iiint \left(\frac{2}{3}\dot{\varepsilon}_{ij}\dot{\varepsilon}_{ij}\right)^{\frac{1}{2}} \mathrm{d}v = \frac{2y_0 t_0}{\sqrt{3}} \iint \left(\dot{\varepsilon}_{\theta z}^2 + \dot{\varepsilon}_{rz}^2\right)^{\frac{1}{2}} \mathrm{d}s, \tag{2}$$

The dissipated power due to the discontinuity can be integrated along the discontinuity surface as

$$\dot{w}_{\mathrm{dis}} = \iint k\left|\Delta v\right| \mathrm{d}s, \tag{3}$$

Accordingly, the total dissipated power due to shear deformation is obtained as

$$\dot{w}_{\mathrm{shear}} = \dot{w}_{\mathrm{dis}} + \dot{w}_f \tag{4}$$

The dissipated power of the deformation zone due to bending and stretching can be determined as

$$\dot{w}_b = \iint M\dot{\mathrm{d}}\phi \mathrm{d}s. \tag{5}$$

$$\dot{w}_s = \iint T\varepsilon_a \dot{\mathrm{d}}l\, \mathrm{d}s = \iint \sigma_a t_0 \varepsilon_a \rho_0 \dot{\mathrm{d}}\emptyset\, \mathrm{d}s \tag{6}$$

where $\dot{\mathrm{d}}\emptyset$ is the change rate of the bending angle in the circumferential direction which could be determined by the travelling angle θ in the $\theta - r$ plane (refer to Li et al., 2014b). Accordingly, the dissipated power due to bending and stretching is

$$\dot{w}_{bs} = \dot{w}_b + \dot{w}_s. \tag{7}$$

To take into account both shear and bending with stretching deformation, a linear combination of these two modules has been constructed to balance the contribution of shear and bending on the prediction of tangential force,

$$\dot{w}_{\text{total}} = \lambda \times \min_{0\le M,N\le 1} \dot{w}_{\text{shear}} + (1-\lambda) \times \min_{0\le M,N\le 1} \dot{w}_{bs}. \quad (8)$$

The above equation for total dissipated power is a function of two optimizing parameters M and N. By minimizing the dissipated power with varying M and N in their defined range (i.e. $0 \le M, N \le 1$), the deformed curved surface for the deformation zone closer to the experiment is obtained. λ is a normalised fraction taking into account parameters of wall angle and step-down size. The purpose of the parameter λ is to weigh the contribution between the shear based model and the bending based model and should be varied with different forming configurations. According to the experimental results as well as the mechanics of plastic deformation, an effective way to determine the value of λ can be achieved by

$$\lambda = \begin{cases} \dfrac{1}{1+\left(\dfrac{\alpha}{90-\alpha}\right)\left(\dfrac{\Delta z}{1-\Delta z}\right)} & (0 < \Delta z \le 1) \\ 0 & (\Delta z > 1) \end{cases} \quad (9)$$

where α and Δz correspond to the algebraic values of the wall angle in degree and step-down size in mm. According to the above equation, the contribution of the shear based model decreases proportionally with the increase of wall angle and step-down size while the significance of bending and stretching rises with more severe plastic deformation due to larger step-down sizes and higher wall angles. It should be noted that the effect of the sheet thickness on the forming force has been considered during the calculation of the dissipated power in both sub-models. In particular, it is assumed that the deformation is entirely taken by bending and stretching modes if the step increment is larger than 1 mm. By this modification, the previous model is enhanced for wider working conditions and is also improved in terms of the adaptability that could be further extended for other shapes. The choice of λ for the combined model will be further discussed in the next section based on the experimental data. Finally, it is reasonably assumed that the rate of plastic work due to the tangential force acting on the forming tool is

$$\dot{w}_{\text{total}} = F_t v_\theta. \quad (10)$$

Substituting the average radius of the deformed zone $(r_i + r_o)/2$ to obtain the angular velocity, the tangential force can be expressed as

$$F_t = \frac{r_i \dot{w}_{\text{total}}}{f \times (r_i + r_o)/2}. \quad (11)$$

4. Experimental validation

To investigate the effects of various forming parameters on the forming forces with different geometries and also the validation of the proposed efficient force prediction model, two shapes of truncated cone and truncated pyramid are selected as the target shapes.

4.1. Experimental setup

The forming tests were performed on a state-of-the-art DLNC-PC (Dieless Numerical Control-PC model) machine dedicated for the ISF process designed by the AMINO® Corporation (Fig. 6(a)). The machine allows a maximum workspace of 2100 mm × 1450 mm × 550 mm to be formed. The movement of the two horizontal axes (X and Y) can have a maximum speed of 60 m/min with a repeatability of ±0.05 mm. The Vertical (Z) axis is driven by an AC servo motor with the power of 1 kW that allows a maximum acting force of 3 kN. Hemispherical tools with diameter values from 10 to 30 mm were used to deform the material. The tip of the tool is tungsten carbide and the body is made of K110 steel which was hardened and tempered to HRC60. The forming tool was set not to rotate in this study for all the tests. The material used in the present study is aluminum 7075-O sheet with various thickness and were cut into 300 mm × 300 mm sized samples.

Before forming, the sheet was clamped on the frame with 12 evenly distributed blank holders. During the forming process, the forming tool is numerically controlled by a FANUC controller which follows the previously designed tool path. The contact between forming tool and metal sheet is lubricated by Shell Tellus Oil 68 to reduce friction and avoid excessive wear of the tool surface. Since the purpose of the current tests is to provide experimental force data for the validation of the proposed analytical model, the forming forces acting on the forming tool have been measured continuously. As shown in Fig. 6(b), a multiple-axis force sensor K6D175-50 was used to measure the forces between the tool and work piece during the forming process. To alleviate the possible deflection from other structures, the force sensor is mounted directly between the spindle and the tool holder. The force sensor is manufactured by ME-Meßsysteme GmbH which allows measuring the three orthogonal forces and three torque components at the same time. The 6-channel output signals are recorded with two NI 9237 data loggers and post-processed with the LabVIEW SignalExpress software.

4.2. Experimental design

In this section, validation of the proposed analytical model is carried out through two benchmark shapes; the truncated cone and truncated pyramid. In particular, during the cone-forming process, four process parameters including step-down size, wall angle, tool diameter and sheet thickness are selected and varied for a comprehensive validation. Additionally, the analytical model is further validated with the experimental results from the forming of truncated pyramids with different step-down size and sheet thickness. A full list of testing parameters for the truncated cone shape is presented in Table 2. Specifically, the effect of wall angle is investigated through tests 1 to 8 by varying wall angle from 30° to 70°. In tests 9 to 17, the Δz is set from 0.1 mm to a large value up to 3 mm to have a full range validation. The effects of tool diameter and sheet thickness are also investigated through tests 18 to 26. All the cones are designed with the same major diameter of 140 mm and a depth of 75 mm (except for tests 1–3 due to the geometric conflict). The successfully formed depths before crack of the material are also recorded in the last column.

For the truncated pyramid shape, the effect of step-down size and sheet thickness are investigated. The wall angle and tool diameter are set at constant values of 55° and 30 mm, respectively. Table 3 summarizes the detailed forming parameters for the pyramid-forming testing.

4.3. Model validation with truncated cone

In the current experimental setup, the forming forces are measured in the Global Cartesian coordinates system which is marked in Fig. 6, so forces need to be converted into tangential and radial directions to make a comparison. The same method presented in Aerens et al. (2010) is used in the current work and the converted forces for a cone with an angle of 65° with a step down of 0.5 mm is shown in Fig. 7. It is observed that the tangential force increases gradually during the early phase of the process and becomes steady for the rest of the process. This steady force is recorded to make comparison with the predicted results calculated with the same

Fig. 6. AMINO incremental forming machine and the implemented force sensor: (a) front view; (b) detailed side view.

parameters presented in Tables 2 and 3 and the model presented in Section 3.

4.3.1. Effect of step-down size

To have a comprehensive assessment of the proposed model, four processing parameters are investigated individually. Previous studies (Aerens et al., 2010; Li et al., 2014c) show that forming forces in the ISF process are largely affected by the value of step-down size. Therefore, it is of great importance to verify that the analytical model is capable of predicting the trend as well as the magnitude accurately for a variation of step down. Fig. 8 presents the comparison between the predicted and measured tangential forces with different step-down sizes ranging from 0.1 mm to 3 mm. It is observed that the prediction provides an accurate result for all the tests except a reasonable deviation (85 N with an error of 12%) for the case with step down of 2 mm. As incorporated in the combined model, the final result is a combination of two sub-models which based on different deformation mechanisms. It is suggested that the

Table 2
Experimental design for truncated cone.

Test no.	Wall angle α (°)	Step down Δz (mm)	Tool diameter (mm)	Thickness (mm)	Feed rate (mm/min)	Designed depth (mm)	Formed depth (mm)
1	30	0.5	30	1.6	4000	28	28
2	40	0.5	30	1.6	4000	40	40
3	50	0.5	30	1.6	4000	60	60
4	60	0.5	30	1.6	4000	75	37.5
5	62	0.5	30	1.6	4000	75	27
6	63	0.5	30	1.6	4000	75	25
7	65	0.5	30	1.6	4000	75	24.5
8	70	0.5	30	1.6	4000	75	23
9	60	0.1	30	1.6	4000	75	29.3
10	60	0.2	30	1.6	4000	75	29.8
11	60	0.3	30	1.6	4000	75	33
12	60	0.4	30	1.6	4000	75	35.2
13	60	0.5	30	1.6	4000	75	37.5
14	60	0.7	30	1.6	4000	75	75
15	60	1.0	30	1.6	4000	75	75
16	60	2	30	1.6	4000	75	75
17	60	3	30	1.6	4000	75	75
18	60	1	10	1.6	4000	75	75
19	60	1	15	1.6	4000	75	75
20	60	1	20	1.6	4000	75	75
21	60	1	25	1.6	4000	75	75
23	60	0.5	30	1	4000	75	35
24	60	0.5	30	2.54	4000	75	75
25	60	1	30	1	4000	75	50
26	60	1	30	2.54	4000	75	75

Table 3
Experimental design for truncated pyramid.

Test no.	Wall angle α (°)	Step down Δz (mm)	Tool diameter (mm)	Thickness (mm)	Feed rate (mm/min)	Designed depth (mm)
1	55	0.5	30	1.02	4000	65
2	55	1	30	1.02	4000	65
3	55	1.5	30	1.02	4000	65
4	55	0.5	30	1.6	4000	65
5	55	1	30	1.6	4000	65
6	55	1.5	30	1.6	4000	65
7	55	0.5	30	2.54	4000	65
8	55	1	30	2.54	4000	65
9	55	1.5	30	2.54	4000	65

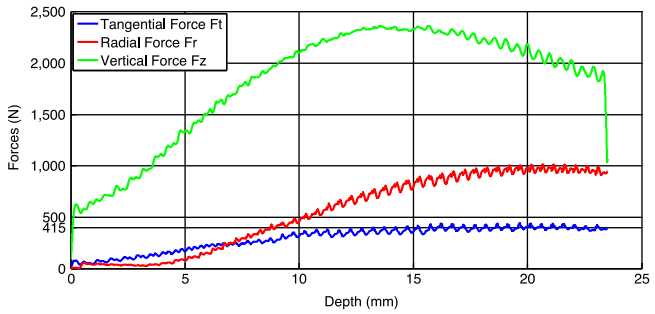

Fig. 7. Converted tangential and radial forces versus forming depth for a cone with an angle of 65° (case 8 in Table 2).

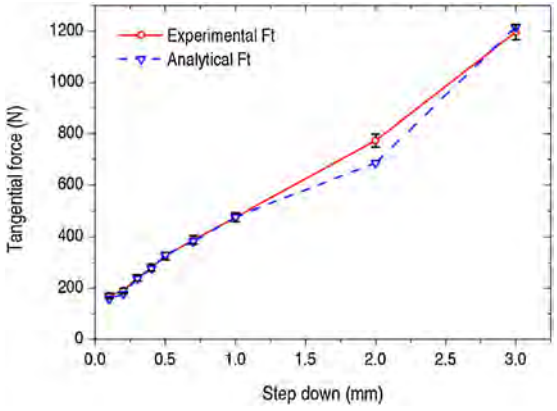

Fig. 8. Comparison between predicted and measured tangential forces with different step-down sizes (r_t = 15 mm, t_0 = 1.6 mm, α = 60°).

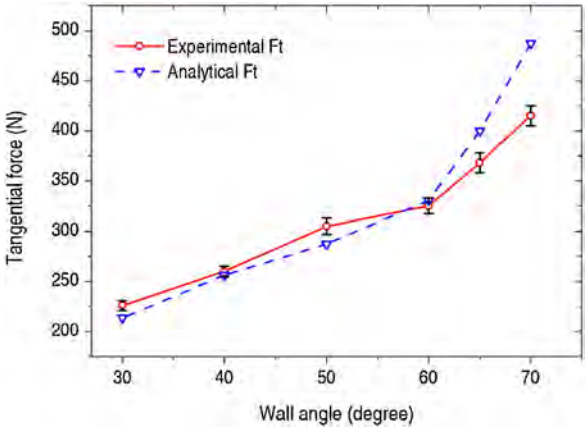

Fig. 9. Comparison between predicted and measured tangential forces with different wall angles (r_t = 15 mm, t_0 = 1.6 mm, Δz = 0.5 mm).

shear deformation could be more significant with small step-down size (i.e. $\Delta z \leq 0.5$ mm), while bending and stretching deformation modes are shown to be dominant when large increments of plastic deformation involves.

4.3.2. Effect of wall angle

The effect of wall angle on the tangential force is also investigated with the range from 30° to 70°. Similar with the effect of step down, the tangential force increases with the increase of wall angle. Comparison between predicted and measured tangential forces with different wall angles is illustrated in Fig. 9. It can be observed that the proposed model underestimates F_t slightly with wall angles smaller than 60° whereas overestimates it at larger wall angles. Specifically, for wall angles below 65°, the average

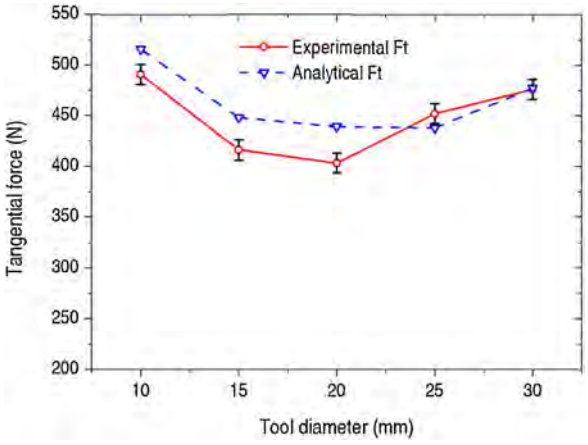

Fig. 10. Comparison between predicted and measured tangential forces with different tool diameter (Δz = 1.0 mm, t_0 = 1.6 mm, α = 60°).

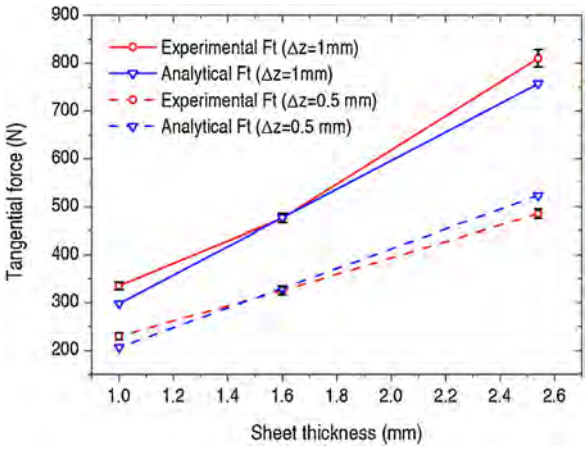

Fig. 11. Comparison between predicted and measured tangential forces with different sheet thickness and step down sizes (r_t = 15 mm, α = 60°).

prediction error could be achieved within 5%. While with the wall angle of 70°, which is close to the maximum formable angle of the material, the effect of strain hardening is more significant which may not be effectively represented by a conventional simplified material constitutive model; therefore, a larger error of 17% with 80 N was obtained.

4.3.3. Effect of tool diameter

Forming tools with different diameter are used in the cone-forming process and the converted tangential forces are shown in Fig. 10. Interestingly, there is a valley effect of the tangential force with the variation of tool diameter from 15 to 30 mm. In the experiments, the minimum force is achieved with a tool diameter of 20 mm and the maximum force occurs for 30 mm. The prediction shows the same trend although the minimum force occurs with the 25 mm tool. Overall, the proposed model reflects the trend of the tangential force with the variation of tool diameter with a deviation less than approximately 10%.

4.3.4. Effect of sheet thickness

In the ISF process, it could be assumed that the tangential force is linearly proportional to the sheet thickness according to Mirnia and Dariani (2012). This assumption is also confirmed by the present experimental work with the forming of the truncated cone. The relations between tangential force and sheet thickness are plotted in Fig. 11 with step-down size of 0.5 and 1 mm. The predicted forces

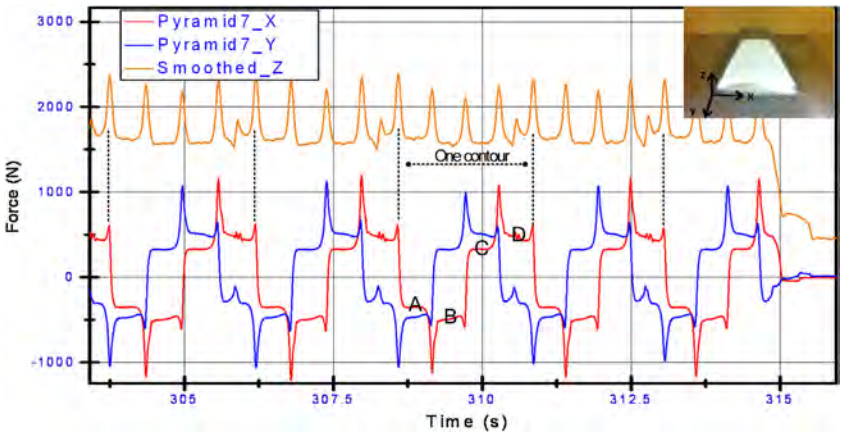

Fig. 12. Three force components in the forming of a truncated pyramid.

based on this analysis are also compared with experimental results. As shown in Fig. 11, in both cases, the predicted forces are in good agreement with the experiments. In particular, a maximum deviation value of 50 N was obtained when forming a 2.54 mm thick material with a step down size of 1 mm.

4.4. Model validation with truncated pyramid

Additionally, the proposed analytical model is verified with the truncated pyramid shape. A typical force trend during the forming of a truncated pyramid is plotted in Fig. 12. It is noticed that there are four stages during each contour which reflects the four sides of the pyramid. Specifically, during one contour as indicated in Fig. 12, the forming force in global X direction undergoes four stages: *A, B, C* and *D*. After the detailed verification of the force variation, it is confirmed that the absolute lower values as marked with stages *A* and *C* correspond to tangential forces. A sample of the formed truncated pyramid is also presented. 9 tests have been performed according to the experimental design in Table 3.

Fig. 13 compares the predicted tangential forces with the experimental values for all the 9 tests. It is shown that, for the experimental results, the tangential force rises with the increase of the step-down size for all the sheets with different thickness. In particular, it is shown that the step down size has more effect on the force when the thickness is larger. It is also confirmed that a larger tangential force is required to deform the thicker sheet. These phenomena are successfully reflected for the tangential forces obtained from the proposed analytical model. As shown in Fig. 13, the relative error between predicted and measured F_t is less than 15% in most of the cases.

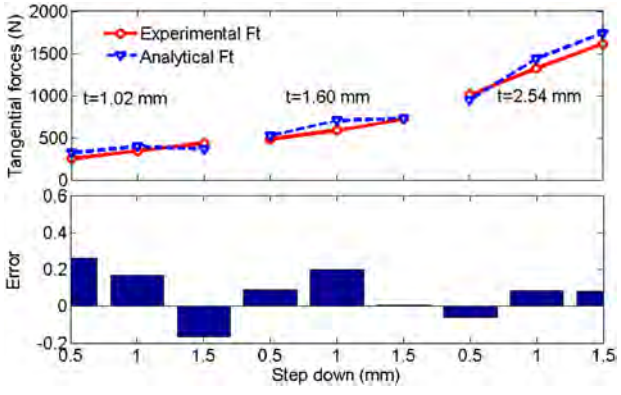

Fig. 13. Comparison between predicted and measured tangential forces with different sheet thickness and step down sizes for the forming of truncated pyramids ($r_t = 15$ mm, $\alpha = 55°$).

5. Model extension

The force prediction model is further generalized to more complex shapes, where wall angle and local radius become a variable rather than a constant. The truncated ellipsoidal cup is designed as a general shape to evaluate the generalized capacity of the analytical model as well as to reveal the fundamental deformation mechanics in the ISF process. The inherent geometric characteristics of this shape make it an ideal benchmark for this process. At a certain contour, both the local radius and wall angle are changing with the moving of the forming tool which is not represented in the previous two shapes. The detailed trend will be discussed in the following section. The studied ellipsoidal cup can be described with an analytical equation by,

$$\frac{x^2}{a^2} + \frac{y^2}{b^2} + \frac{z^2}{c^2} = 1. \tag{12}$$

The ellipsoidal cup can also be written as a parametric equation by

$$\begin{aligned} x &= a \cos u \sin v \\ y &= b \sin u \sin v \\ z &= c \cos v \end{aligned} \tag{13}$$

where $a = 75$ mm, $b = 45$ mm, $c = 60$ mm, and $u \in [0, 2\pi]$ and $v \in [0, \pi]$. To ensure the successful forming of the ellipsoidal cup, only a part of the shape will be formed due to the following considerations. First, due to the limitation of formability, the region with excessive wall angles should be avoided. Also, as the forming tool will be contacting with the inner surface, the inner local radius of the shape should be larger than the tool radius to avoid geometric conflict. As a result, the ellipsoidal shape has been truncated between the planes of $z = -20$ and $z = -50$ and the detailed dimensions are shown in Fig. 14. Two tests with different step-down sizes are designed for this shape as listed in Table 4.

Fig. 15 plots the experimentally measured forces of 3 orthogonal directions for the last ten forming contours with a step down of 1 mm. During this period, it can be seen that forces have reached a relative steady state with the same pattern and magnitude for each contour. Specifically, the forces in the horizontal plane (F_x and F_y) present a symmetric pattern about zero. During the forming between points *a* and *c* (refer to Fig. 14), both magnitudes of horizontal forces experienced a sinusoidal-like decrease-increase changing process. F_x drops sharply to zero and then reaches the negative peak value at the point of *c*. However, F_y hasn't decreased

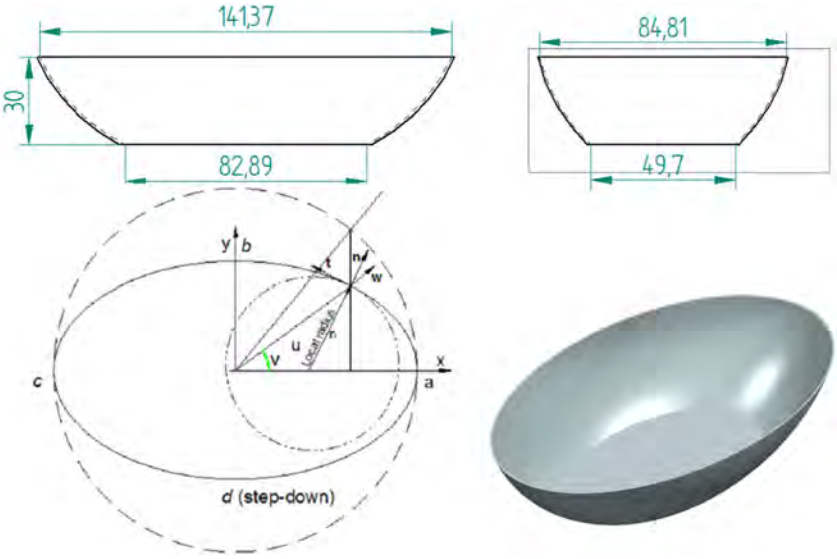

Fig. 14. Dimensions of the truncated ellipsoidal cup and the sketch of an ellipsoidal contour.

Table 4
Experimental design for truncated ellipsoidal cup.

Test no.	Step down Δz (mm)	Tool diameter (mm)	Thickness (mm)	Feed rate (mm/min)	Designed depth (mm)
1	0.5	30	1.6	4000	30
2	1	30	1.6	4000	30

to zero until reaching the point of *c*. In terms of vertical force F_z, it only fluctuates over a limited range during each loop of the forming process and the steady value is recorded as 2100 N.

The tangential force F_t is obtained using the similar conversion method mentioned in the cone-forming process. Fig. 16 plots the converted tangential force during two contours of a forming case with an ellipsoidal cup. Unlike the previous results for both truncated cone and pyramid, the tangential force is not steady within one contour but changing with a regular pattern. Specifically, the lowest tangential force occurs before the end points of the long axis (points *a* and *c* in Fig. 14), and then increases to the peak value at a certain point (where angle *u* is about 30°) before dropping continuously to the smallest value before point *c*. This trend is also presented in the other half of the ellipse except for a sudden dip resulting from the step-down movement of the forming tool.

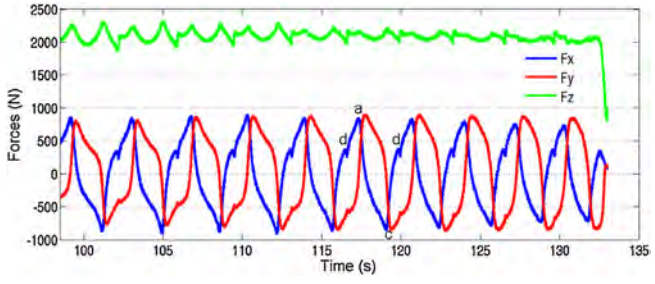

Fig. 15. Force trend during the forming of ellipsoidal cup ($\Delta z = 1$ mm, $t = 1.6$ mm).

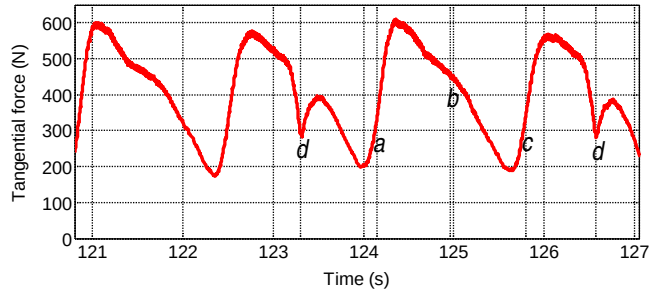

Fig. 16. Converted tangential force from experimental tests for ellipsoidal cup with a step-down size of 1 mm.

As discussed previously, in the ellipsoidal cup-forming process, both the local radius and wall angle are constantly changing over time. As a result, the metal sheet undergoes an additional twisting deformation. Therefore, the model has to be generalized by taking into account these effects. Accordingly, at a particular point during ellipsoidal cup-forming process as marked in Fig. 14, the twist in the local coordinates (*ntw*) is given by Timoshenko and Woinowsky-Krieger (1959),

$$\frac{1}{T_{nt}} = \frac{\partial^2 w}{\partial n \partial t} = \frac{\partial \frac{\partial w}{\partial n}}{\partial t} = \frac{\partial \alpha}{\partial t}, \tag{14}$$

where *w* is the displacement normal to the mid-surface of the plate and *t*,*n* are defined as the forming and normal direction, respectively. α is the wall angle in the normal direction at a particular point on the contour and its variation is shown in Fig. 17. It is noted from the above equation that the change rate of wall angle along the tangential direction can be treated as an indicator to reflect the effect of twisting. The twist does plastic work and therefore affects the forming force. This can be taken into account empirically by modifying the analytical model with the effect of change rate of wall angle and local radius r_l as follows:

$$F_{t\_new} = \left(1 + 2r_l \frac{\partial \alpha}{\partial t}\right) \times F_t = \left(1 + 2\frac{\partial \alpha}{\partial u}\right) \times F_t \tag{15}$$

where F_t is the predicted value from original combined model and a scaled factor of 2 is used to rectify the amplitude of the variation. $\partial\alpha/\partial u$ represents the rate of change of wall angle over the angle *u* defined in Eq. (13) and its variation during one contour is demonstrated in Fig. 17. Note this modification is not in conflict

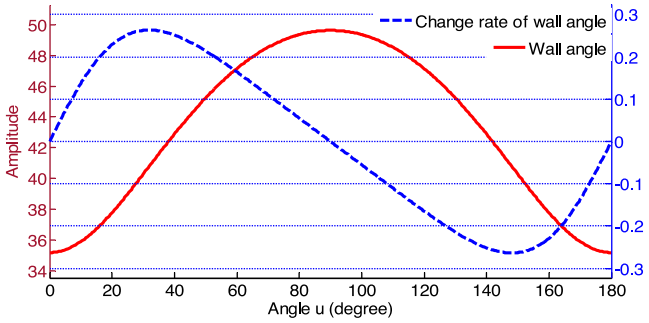

Fig. 17. The variations of the wall angle and its change rate over angle *u*.

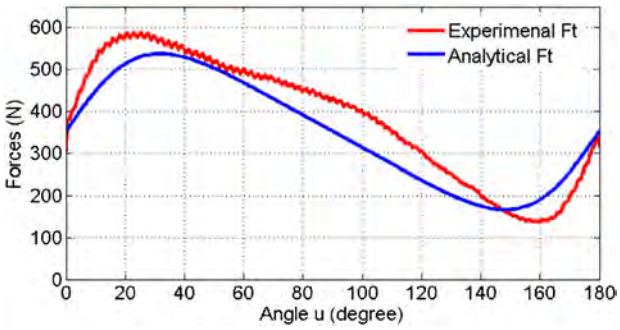

Fig. 18. Predicted tangential force for ellipsoidal cup with a step-down size of 1 mm.

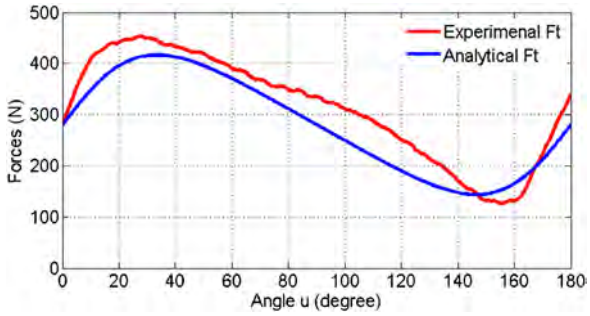

Fig. 19. Predicted tangential force for ellipsoidal cup with a step-down size of 0.5 mm.

with verification for the truncated cone and pyramid in which the wall angle at each step is constant so the change rate is zero.

The predicted tangential forces are compared with the converted one in Figs. 18 and 19 with step-down size of 1 mm and 0.5 mm, respectively. It is observed that the predicted values are in good agreement with the experimental results and deviations are also within a reasonable range. In particular, the positions of both maximum and minimum values are correctly predicted and also the overall amplitude during the whole contour is reasonably represented. Further study is necessary to develop a less empirical model.

The above results reflect that the extended model has been validated through a specific shape but it is still limited by the integrity of experimental tests. Since it has been clearly demonstrated that the trend of the measured tangential force is closely related to the feature of the local geometry, further in-depth theoretical justification of the effect of twisting on the plastic dissipated power could be incorporated into the model as a potential approach to mitigate such a limitation. As discussed, the choice of an ellipsoidal cup shape is due to the continuous variation of both wall angle and local radius during one contour. In addition, the available symbolic expression of the geometry further allows an efficient verification procedure for the empirical correlation. Although the shape of an ellipsoidal cup may be still considered as an extension of truncated cone and pyramid, the current model provides valuable foundation for future investigation towards more general shapes. Another suggestion for the future work is to investigate the influence of the material type on the tangential force, using the proposed model.

6. Conclusions

In the present work, a comprehensive FE model with fine solid elements is established and deformation behaviors of typical elements after deformation are analyzed. These provide further insights into the deformation mechanism and more evidence for the derivation of the analytical model. Based on the deformation analysis, an efficient tangential force prediction model is deduced which considers main deformation modes including shearing, stretching and bending. In particular, the contribution from each deformation mode is related to the variation of forming parameters. Additionally, comprehensive experimental tests with shapes of truncated cone, truncated pyramid by varying the critical forming parameters are conducted to investigate the effects of process parameters on forming forces. The predicted tangential forces from the proposed model are then compared with those experimental results and good agreements are obtained. Finally, the analytical model is further extended to investigate its potential capacity to handle complex geometries (e.g. ellipsoidal cup). The conclusions can be summarized as follows:

- It is confirmed from FE simulation that the deformation in ISF process is a combination of shearing, bending and stretching. Specifically, direct strain in perpendicular to the forming direction (ε_{11}) is the major deformation mode in the cone-forming process. The strain ε_{11} could be accumulated to a large value while strain in the forming direction only alternates at smaller values. Shear strain in the forming direction (ε_{23}) prevails greatly among the three shear components and the maximum value occurred at the middle of the sheet. It is also found that the in-plane shear strain is not negligible, especially at the upper surface.
- The proposed force prediction model is validated through a comprehensive experimental campaign with two geometric shapes (truncated cone and truncated pyramid) and various process parameters (step down, wall angle, tool radius and thickness). It is concluded that the tangential force increases with the increase of step-down, wall angle and sheet thickness. However, the tangential force varies in a concave manner with the variation of tool diameter from 10 to 30 mm with a minimum occurring between 20 and 25 mm.
- The proposed analytical model is further extended to capture the changing of local curvature and wall angle during forming to address more complex shapes. The truncated ellipsoidal cup is selected as the target shape which has local curvature and wall angle variations in each contour. The modified model is able to predict reasonably accurate tangential force variation in each contour compared to experiments.

It is also worthwhile to point out that the current analytical model has its limitations and future work is needed to extend its adaptability. The combined model is semi-analytical and there is still uncertainty as to the type of deformation mode that is dominant in the ISF process under different forming configurations. As a further contribution, the extended model shows great potential towards dealing with more complex geometries, although further theoretical justification is essential. Considering the proposed model can be efficiently solved within several minutes, the further

development of this model will greatly facilitate the production design and optimization process in ISF.

Acknowledgements

The present work was supported by Australian Research Council (ARC) Linkage project (LP100200689), Boeing Research and Technology Australia and QMI Solutions in Australia. China Scholarship Council (CSC) is also acknowledged for the scholarship support.

Appendix A

In the present model, as shown in Fig. 5(c), the deformation zone is divided into three regions: I contact region, II non-contact region following the height of tool head and III non-contact region following the height of the formed sheet. One of the typical flow lines with a radius of r is depicted in Fig. 5(b). The flow line is defined as three curves Zf_c, f_t and Zf_s which correspond to region I, II and III, respectively. Zf_c has the same geometric function with the tool head surface as it is the region contacting with the tool but the conjunct point with Zf_t is unknown therefore is advisable to be determined as the following equation with an adjustable parameter M,

$$Zf_c\left(r,\theta\right) = Z_c = M\left(Z_s - Z_o\right) + Z_o, \qquad (0 \le M \le 1) \tag{A1}$$

where Z_s and Z_o are the vertical position of the sheet formed in previous pass and the tool vertex with the radius of r. To represent the height variation of the non-contact surface of the sheet, a normalized shape function $S(X)$ is introduced. $S(X)$ is tentatively designed as 2 s order Bezier curves with the following equation,

$$S(X) = \left\{ \begin{array}{ll} 1 - \left(\dfrac{\theta - \theta_c}{\theta_t - \theta_c}\right)^2 (1-N)\left(\dfrac{r_o - r}{r_o - r_i}\right) & \theta_c \le \theta \le \theta_t \quad 0 \le N \le 1 \\ 1 - \left(\dfrac{\theta - \theta_s}{\theta_s - \theta_t}\right)^2 (1-N)\left(\dfrac{r_o - r}{r_o - r_i}\right) & \theta_t \le \theta \le \theta_s \quad 0 \le N \le 1 \end{array} \right\}. \tag{A2}$$

here N is another adjustable parameter which can be obtained through the optimisation of the dissipated power. The value of $S(X)$ changes from N to 1 corresponding to the variation of θ and r within their ranges.

References

Aerens, R., Eyckens, P., Van Bael, A., Duflou, J.R., 2010. Force prediction for single point incremental forming deduced from experimental and FEM observations. Int. J. Adv. Manuf. Technol. 46, 969–982.

Allwood, J.M., King, G.P.F., Duflou, J., 2005. A structured search for applications of the incremental sheet-forming process by product segmentation. Proc. Inst. Mech. Eng. Part B J. Eng. Manuf. 219, 239–244.

Ambrogio, G., De Napoli, L., Filice, L., Gagliardi, F., Muzzupappa, M., 2005. Application of incremental forming process for high customised medical product manufacturing. J. Mater. Process. Technol. 162–163, 156–162.

Ambrogio, G., Filice, L., Micari, F., 2006. A force measuring based strategy for failure prevention in incremental forming. J. Mater. Process. Technol. 177, 413–416.

Duflou, J., Tunçkol, Y., Szekeres, A., Vanherck, P., 2007. Experimental study on force measurements for single point incremental forming. J. Mater. Process. Technol. 189, 65–72.

Emmens, W.C., Boogaard, A.H., 2008. An overview of stabilizing deformation mechanisms in incremental sheet forming. J. Mater. Process. Technol. 209, 3688–3695.

Eyckens, P., Belkassem, B., Henrard, C., Gu, J., Sol, H., Habraken, A.M., Duflou, J.R., Van Bael, A., Van Houtte, P., 2011. Strain evolution in the single point incremental forming process: digital image correlation measurement and finite element prediction. Int. J. Mater. Form. 4, 55–71.

Filice, L., Ambrogio, G., Micari, F., 2006. On-line control of single point incremental forming operations through punch force monitoring. CIRP Ann. Manuf. Technol. 55, 245–248.

Fiorentino, A., 2013. Force-based failure criterion in incremental sheet forming. Int. J. Adv. Manuf. Technol. 68, 557–563.

Hosford, W., Caddell, R., 2007. Metal Forming: Mechanics and Metallurgy. Cambridge University Press, Cambridge.

Ingarao, G., Ambrogio, G., Gagliardi, F., Di Lorenzo, R., 2012. A sustainability point of view on sheet metal forming operations: material wasting and energy consumption in incremental forming and stamping processes. J. Cleaner Prod. 29–30, 255–268.

Iseki, H., 2001. An approximate deformation analysis and FEM analysis for the incremental bulging of sheet metal using a spherical roller. J. Mater. Process. Technol. 111, 150–154.

Jackson, K., Allwood, J., 2009. The mechanics of incremental sheet forming. J. Mater. Process. Technol. 209, 1158–1174.

Johnson, W., Mellor, P.B., 1983. In: Horwood, E. (Ed.), Engineering Plasticity. Ellis Horwood Limited, Van Nostrand Reinhold (UK) Ltd., New York, Chichester, West Sussex, England.

Li, Y., Liu, Z., Daniel, W.J.T., Meehan, P.A., 2014a. Simulation and experimental observations of effect of different contact interfaces on the incremental sheet forming process. Mater. Manuf. Processes 29, 121–128.

Li, Y., Liu, Z., Lu, H., Daniel, W.J.T., Liu, S., Meehan, P., 2014b. Efficient force prediction for incremental sheet forming and experimental validation. Int. J. Adv. Manuf. Technol. 73, 571–587.

Li, Y., Liu, Z., Lu, H., Daniel, W.J.T., Meehan, P.A., 2014c. Experimental study and efficient prediction on forming forces in incremental sheet forming. Adv. Mater. Res. 939, 313–321.

Liu, Z., Li, Y., Meehan, P., 2013. Experimental investigation of mechanical properties, formability and force measurement for AA7075-O aluminum alloy sheets formed by incremental forming. Int. J. Precis. Eng. Manuf. 14, 1891–1899.

Lu, B., Fang, Y., Xu, D.K., Chen, J., Ou, H., Moser, N.H., Cao, J., 2014. Mechanism investigation of friction-related effects in single point incremental forming using a developed oblique roller-ball tool. Int. J. Mach. Tools Manuf. 85, 14–29.

Micari, M.G., Duflou, J., Shirvani, B., Clarke, R., Di Lorenzo, R., Fratini, L., 2007. Incremental forming process for the accomplishment of automotive details. Key Eng. Mater. 344, 559–566.

Mirnia, M.J., Dariani, B.M., 2012. Analysis of incremental sheet metal forming using the upper-bound approach. Proc. Inst. Mech. Eng. Part B J. Eng. Manuf. 226, 1309–1320.

Petek, A., Kuzman, K., Suhač, B., 2009. Autonomous on-line system for fracture identification at incremental sheet forming. CIRP Ann. Manuf. Technol. 58, 283–286.

Raithatha, A., Duncan, S., 2009. Rigid plastic model of incremental sheet deformation using second-order cone programming. Int. J. Numer. Methods Eng. 78, 955–979.

Silva, M.B., Skjoedt, M., Martins, P.A.F., Bay, N., 2008. Revisiting the fundamentals of single point incremental forming by means of membrane analysis. Int. J. Mach. Tools Manuf. 48, 73–83.

Smith, J., Malhotra, R., Liu, W.K., Cao, J., 2013. Deformation mechanics in single-point and accumulative double-sided incremental forming. Int. J. Adv. Manuf. Technol. 69, 1185–1201.

Timoshenko, S., Woinowsky-Krieger, S., 1959. Theory of Plates and Shells. McGraw-Hill, New York, US.